Sensors & Diagnostics

TUTORIAL REVIEW

View Article Online
View Journal | View Issue

Cite this: *Sens. Diagn.*, 2024, **3**, 203

A nIR fluorescent single walled carbon nanotube sensor for broad-spectrum diagnostics

Minyeong Yoon, †[a] Yullim Lee, †[a] Seungju Lee, [a] Youngwook Cho, [a] Damee Koh, [a] Seyoung Shin, [a] Changyu Tian, [a] Youngho Song, [a] Joohoon Kang [b] and Soo-Yeon Cho *[a]

Received 27th September 2023,
Accepted 19th December 2023

DOI: 10.1039/d3sd00257h

rsc.li/sensors

Detecting chemical and biological molecules that indicate diseases is a prerequisite technology for the efficient diagnoses and treatment of aging and diseases in living organisms. A variety of nanoscale sensor materials have been extensively utilized in various diagnoses with their strength in sensitivity. Among them, near-infrared (nIR) fluorescent single-walled carbon nanotubes (SWCNTs), especially, have shown attractive properties for powerful diagnostics as they can ensure sufficient spatial, temporal, or molecular resolution, tissue transparent fluorescence, and high selectivity based on a wide range of surface functionalization techniques. This review provides a comprehensive overview of recent nIR fluorescent SWCNT nanosensor design for versatile diagnostic applications. We discuss how the nIR fluorescence of SWCNTs can be utilized more efficiently in each diagnostic situation based on distinct SWCNT interfacing strategies including direct biofluid sensing, hydrogel implantation, and direct injection into the targets. Finally, we provide a summary of the diagnostic performance and target diseases of SWCNT based nIR sensors and an outlook on opportunities for possible future research directions.

1. Introduction

Accurate and rapid diagnosis of diseases is the most important technology for the effective treatment of patients. Conventional diagnosis has primarily relied on clinical manifestations such as fever, pain, swelling, headache, or neurological symptoms, *etc.* However, given a mass of overlapping symptoms across various diseases, this approach often poses challenges in making accurate and rapid determinations. Detecting specific chemical and biological molecules related to diseases can overcome these limitations of ambiguity. Recent development of materials science and nanotechnology has provided a powerful diagnostic platform based on biomarker detection.[1] A variety of sensing materials including organic and inorganic low-dimension materials

[a] *School of Chemical Engineering, Sungkyunkwan University, Suwon 16419, Republic of Korea. E-mail: sooyeonc@skku.edu*
[b] *School of Advanced Materials Science and Engineering, Sungkyunkwan University, Suwon 16419, Republic of Korea*
† These authors contributed equally to this work.

Minyeong Yoon

Minyeong Yoon received her B.S. degree in Chemical Engineering from Sungkyunkwan University (SKKU), in 2023. She is currently a Ph.D. candidate in Chemical Engineering at SKKU. Her research interests include optoelectrical nanosensors for biomarker detection, synthesis of artificial antibodies, and integrated nanosensor system design for diagnostics and biomonitoring.

Yullim Lee

Yullim Lee received her B.S. degree in Chemical Engineering from Sungkyunkwan University (SKKU) in 2022. She is currently a Ph.D. candidate in Chemical Engineering at SKKU. Her research interests include diagnostic biochemical nanosensor systems.

have been researched and developed for diagnostics by structure and surface modification to enhance the sensitivity and selectivity for the target biomarkers. Electrical, optical, and mechanical properties of the sensing materials are converted to diagnostic signals for on-site users when a biomarker interacts with the sensor materials.[2]

Single-walled carbon nanotubes (SWCNTs), in particular, are an attractive sensor material candidate for various diagnostic applications due to their unique optical properties. A SWCNT is a long wrapped graphene sheet having one-dimensional (1D) structure, classified by a chiral index meaning the roll-up vector of the sheet. These chiralities affect the density and energy of electronic states of SWCNTs, causing them to exhibit metallic, semi-metallic, or semiconducting characteristics, and consequently determine optoelectronic properties.[3] SWCNTs possess E11 and E22 bandgap structures and generate electron–hole pairs, known as excitons, which can diffuse along their axis, when they are excited with light.[4] In particular, semiconducting SWCNTs induce excitation to E22 upon absorption of visible light.[5,6] Through the subsequent rapid decay to E11 and radiative recombination, semiconducting SWCNTs emit near infrared (nIR) fluorescence ranging from 800 to 1400 nm with visible light stimulation.[7,8] This nIR signal from SWCNTs shows robustness for biomedical imaging applications compared to conventional organic fluorescent dyes due to their resistance to photobleaching and tissue transparency achieved by fluorescence between blood and water absorption in the visible and infrared region, which facilitates the real-time and non-invasive *in vivo* diagnostics based on spatiotemporal information.[6] This is hard to achieve with electrical, electrochemical, or mechanical sensor materials.[9–11] In addition, their 1D carbon nanostructure with a large surface-to-volume ratio significantly enhances sensitivity to target molecular recognitions and enables various surface functionalization methods including non-covalent and covalent strategies for molecular selectivity control (Fig. 1a). With these strengths, a facile sensing strategy based on nIR fluorescent SWCNTs called corona phase molecular recognition (CoPhMoRe) has been introduced.[12] SWCNTs construct distinct three-dimensional (3D) nanointerface complexes according to the hydrophilicity and hydrophobicity of polymeric excipients encapsulating the SWCNT surfaces, which can selectively recognize target analytes. The SWCNT–analyte interaction can lead to Fermi level shift, changes in fluorescence intensity, or solvatochromic shift (Fig. 1b).[13]

When antibodies or receptors specific to a biomarker are covalently attached to SWCNTs, the resulting substances can serve as sensitive, selective, and solid nanosensors. Here, sp^3 quantum defects of SWCNTs can sense metal ions or protons themselves as well as efficiently serve as versatile anchors for bioconjugation in specific nanosensor development.[14–16] In addition, various non-covalent surface functionalization techniques with DNA or polymers can also produce versatile nanosensor surfaces, which accelerates the assay development process. For example, sensitive detection of DNA or micro RNA can be achieved by non-covalent wrapping of a single DNA oligonucleotide containing a nanotube-binding sequence and miRNA capture sequences.[17,18] These attractive sensing properties of a SWCNT transducer can be efficiently utilized for diagnostic application by integration with sensor devices such as microchips, substrates, or fiber optics.[19] The device then detects small molecules, nucleic acids, proteins, or pathogens in biofluid and enables direct sensing of the biomarkers without further sensor implantation (Fig. 1c).[20,21] Real-time *in vivo* diagnosis can be achieved with development of a biocompatible substrate such as hydrogel that can contain SWCNT sensors under humid conditions, and direct the injection technique of SWCNTs into living organisms (Fig. 1d). Starting from a mouse model, the field of application of these biomaterials and sensing devices has now expanded greatly to animals, marine life, and even plants.

Despite being applied to such a variety of diagnostic applications based on unique optical properties, there has been no comprehensive technological review of SWCNT sensor based diagnostic applications and material interfacing strategies so far. This review will summarize recent strategies about direct biofluid sensing, hydrogel implantation, and nanosensor injection for diagnostic applications using the unique optical sensing characteristics of nIR fluorescent SWCNTs. It will also suggest directions for future technological development of SWCNT sensors for real-world diagnostic applications.

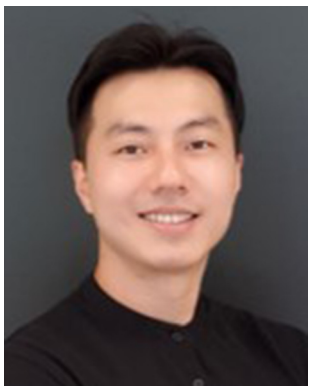

Soo-Yeon Cho

Soo-Yeon Cho is an assistant professor at Sungkyunkwan University (SKKU), School of Chemical Engineering. He received his B.S. (2013) and Ph.D. (2019) from the Department of Chemical and Biomolecular Engineering at KAIST. He worked as a postdoctoral associate at MIT Chemical Engineering from 2019 to 2022 and he joined SKKU. His research focuses on advanced biochemical analytics using fluorescent nanosensor technology and AI software.

2. Direct biofluid sensing using SWCNTs

Many sensor materials are often used *in vitro* only due to the lack of selectivity and sensitivity, requiring direct interfacing of the sensor materials with the source of the disease from which the biomarker originates.[22] Since SWCNT-based sensors provide selective molecular recognition sites and sensitive nIR fluorescence variations at the same time, they

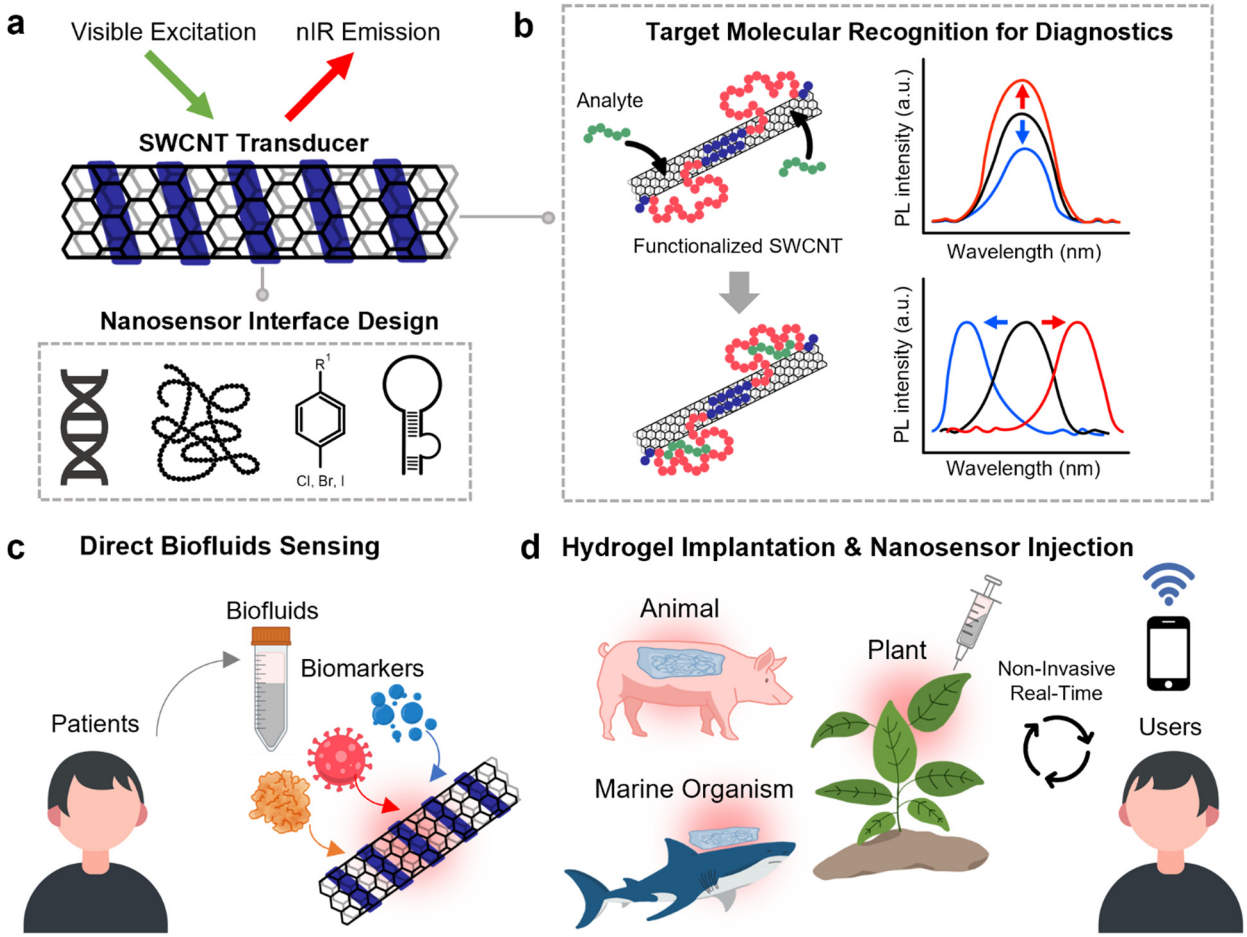

Fig. 1 Schematics of broad-spectrum diagnostics using nIR fluorescent SWCNT sensors. (a) SWCNT sensor construct based on interface design. (b) Molecular recognition mechanism of a SWCNT based on fluorescent spectrum variations. (c) Direct biofluid sensing approach of SWCNT nanosensors. (d) Hydrogel implantation and direct injection approach of SWCNT nanosensors.

can be used for direct sensing of biomarkers from biofluids such as blood, serum, tears, sweat, or saliva that have been taken from the human body. In order to use SWCNTs for direct biofluid sensing, there is a significant need for practical designs capable of providing selectivity towards diverse biomarker molecules within the dynamic compositions of biofluids. SWCNTs are promising candidates for direct biofluidic sensing transducers, owing to the extensive array of functionalization possibilities for the carbon surface and the inherent robustness of the materials.

Diagnosis based on direct biofluid sensing has been conducted by either mixing analytes into a synthesized SWCNT nanosensor solution and observing changes in nIR fluorescence spectrum intensity or by dropping the analyte onto a substrate coated with a SWCNT. By pre-screening of the SWCNT library for selectivity towards specific biomarkers in biofluids, it allows user to immediately diagnose diseases by detecting signal changes. Budhathoki-Uprety *et al.* recently developed an albumin sensor using SWCNT fluorescence for the rapid detection of microalbuminuria, a critical clinical marker associated with various diseases including diabetes, hypertension, cardiovascular diseases, and cancer (Fig. 2a).[23–26] The SWCNT was functionalized with encapsulation of polycarbodiimide (PCD) polymer, which was designed to mimic fatty acid binding to albumin based on the crystal structure.[26] The PCD-SWCNT complexes showed distinct nIR fluorescence spectra to albumin in the microalbuminuria range with both an increase in intensity and a hypsochromic shift. The nanosensor shows limit-of-detection (LOD) down to 3 mg L^{-1}, which is comparable to typical sensitivity of immunoturbidimetry assay (1 mg L^{-1}). Interfering proteins such as transferrin, γ-globulins, and degraded albumin produced either minimal alteration or exhibited a bathochromic shift instead of hypsochromic shift in nanotube emission, enhancing the specificity of the biofluidic diagnostic conditions. In addition, practical testing in human patients with microalbuminuria demonstrated the reliability and efficiency of the SWCNT nanosensor when applied to real clinical urine samples. To explore broader application, the functionality of the SWCNT nanosensor was examined in a solid scaffold suitable for application and dried onto surfaces, resulting in an acrylic-based mixture that preserved sensing capability. Consequently, a self-sustaining optical sensor paint emerged, enabling the assessment of microalbuminuria in patient samples. A deeper investigation into these nIR shifts

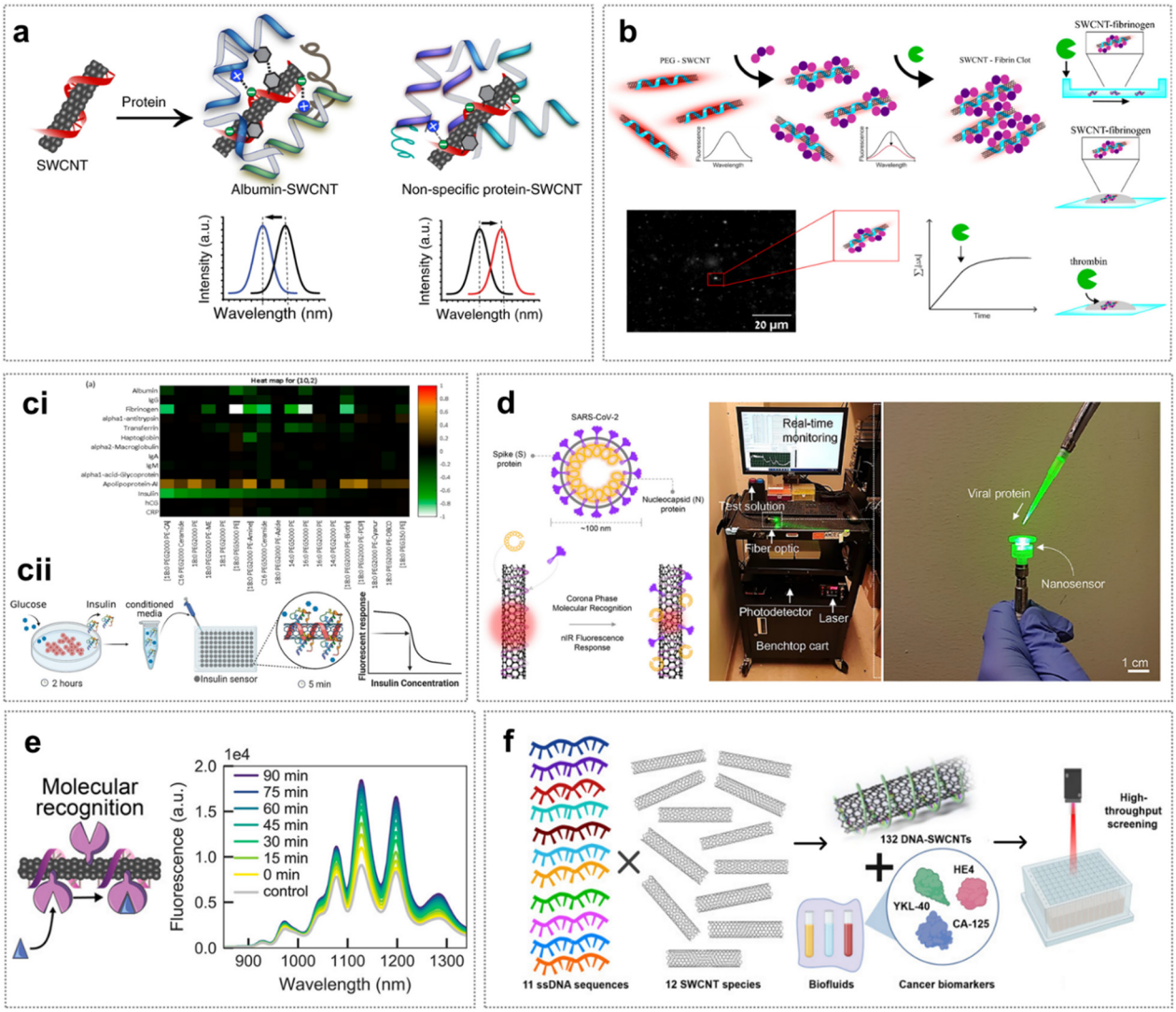

Fig. 2 Direct biofluid sensing of SWCNTs for diagnostics applications. (a) PCD/SWCNT detects albumin by hypsochromic shift to diagnose microalbuminuria. Reprinted with permission from ref. 26. Copyright 2022 Springer Nature. (b) DPPE–PEG/SWCNT for fibrin clotting imaging and monitoring. Reprinted with permission from ref. 27. Copyright 2023 American Chemical Society. (ci) nIR fluorescence signal heatmap of a PEG/SWCNT sensor array to detect insulin for diagnosis of diabetes mellitus. Reprinted with permission from ref. 31. Copyright 2018 American Chemical Society. (cii) PEG/SWCNT array detects insulin through emitted nIR change. Reprinted with permission from ref. 33. Copyright 2021 John Wiley & Sons. (d) Recognition of SARS-CoV-2S and N protein by a PEG-lipid/SWCNT nanosensor in saliva. Reprinted with permission from ref. 34. Copyright 2021 American Chemical Society. (e) SWCNT functionalized with ACE2 to detect SARS-CoV-2S protein. Reprinted with permission from ref. 35. Copyright 2021 American Chemical Society. (f) Perception-based DNA-SWCNT nanosensor platform acquired through machine learning to detect a gynecologic cancer biomarker. Reprinted with permission from ref. 36. Copyright 2021 American Association for the Advancement of Science.

with mechanistic studies could yield valuable insights into the distinct sensitivity and operational principles of the nanosensors, potentially leading to significant advancements in sensor design and functionality.

Blood coagulation plays a crucial role in the defence mechanism against excessive bleeding when a blood vessel is damaged. It is possible to diagnose coagulation disorders and blood clotting-related conditions by sensing the formation of fibrin clots during the blood coagulation process. Gerstman *et al.* have developed a SWCNT based sensing platform to monitor and image fibrin clotting in real-time (Fig. 2b).[27] Fibrinogen undergoes polymerization and forms fibrin clots with thrombin exposure. The unique structural characteristics of dipalmitoylpho-sphatidylethanolamine (DPPE)–poly(ethylene glycol) (PEG) (5000) corona formed upon adsorption onto the SWCNT surface, along with the distinctive structure of fibrinogen, are hypothesized to play a crucial role in molecular recognition. The 3D structure of fibrinogen, coupled with the 1D structure of SWCNTs, allows multiple binding sites on the protein to be near the SWCNT corona, simultaneously. This interaction is anticipated to be pivotal in the molecular recognition process.[28] The diagnostic approach using SWCNTs for fibrinogen and thrombin differs from conventional methods such as PT (prothrombin time) and APTT (activated partial

thromboplastin time) tests, as it provides dynamic information throughout the cascade, allowing for the assessment of the coagulation process. The SWCNT is functionalized with DPPE–PEG to detect fibrinogen by screening assay, which showed fluorescence intensity decrease depending on fibrinogen concentrations.[28] It is noticeable that the fluorescence emission of DPPE–PEG/SWCNT remains unaffected by the addition of thrombin. However, DPPE–PEG/SWCNT becomes part of the fibrin clots enabling their visualization through two-dimensional (2D) nIR fluorescent imaging, which offers spatiotemporal information about the clotting process for the users. Furthermore, single bundle SWCNT tracking reveals a gradual slowdown of SWCNT diffusion during the fibrin polymerization process, with the rates being influenced by both fibrinogen and thrombin concentrations.[27] This strategy utilizing DPPE–PEG/SWCNT enables the evaluation of the coagulation process, offering real-time insights throughout the cascade. It can contribute to blood coagulation research and promote the development of innovative diagnostic tools of blood coagulation.

The detection of insulin is essential for diabetes diagnostics as it preserves the blood glucose level.[29] In contrast to glucose, which can be easily monitored continuously or sampled by the patient whenever needed, insulin levels are currently not accessible through a continuous monitoring system so far.[30] Bisker *et al.* designed 18 arrays of PEG-lipid conjugated SWCNTs for selective insulin detection (Fig. 2ci).[31] Among the array, C16 PEG(2000 Da)-ceramide-SWCNT induces 62% reduction in nIR fluorescence intensity in the presence of insulin. The corona phase of C16PEG(2000 Da)-ceramide-SWCNT showed no priority affinity towards insulin, which was examined by comparison of isothermal titration calorimetry of heat released from phosphate-buffered saline (PBS) and insulin solution. The sensor provides the current detection range exceeding the physiological insulin concentration of 57–79 pM during fasting and extending up to 430 pM after meals. Hence, this nanosensor construct can be efficiently utilized in practical diagnosis if the sensitivity is optimized further.

As a following work, Ehrlich *et al.* compared SWCNT sensors for insulin using two different types of surface functionalization (Fig. 2cii).[33] The first method is using a natural insulin aptamer and the second method is using C_{16}-PEG(2000 Da)-ceramide following previous research. Although both sensors showed significant quenching response to insulin, the response of C_{16}-PEG(2000 Da)-ceramide-SWCNT is more stable and reproducible since the polymer chain forms solid 3D interfaces for molecular recognition. This PEG based SWCNT nanosensor can be used in a microenvironment of intact pancreatic islets or in the proximity of an insulin injection site, which shows promising effectiveness for the diagnosis of diabetes.[32,33]

Detection of viral components including antigens, antibodies, and nucleic acids is one of the major parts of diagnostics. To effectively combat the spread of contamination, a simple yet rapid and effective detection technology is essential. Development of SWCNT-based nanosensors has been recently started for rapid virus detection and diagnosis since the Coronavirus disease 2019 (COVID-19) pandemic. Cho *et al.* developed an artificial antibody-based infectious disease diagnostic technology using the PEG-lipid corona phase of SWCNTs, which allows sensing of SARS-CoV-2 antigens without the need for any antibodies or receptors (Fig. 2d).[34] To detect SARS-CoV-2 proteins, PEG-lipids capable of forming an extensive surface corona were employed, by manipulating the molecular weight and chain length to induce the differences in shape and electronic potential of the corona interfaces. A nanosensor library of PEG-lipid-wrapped SWCNTs was created by incorporating PEG chains of varying lengths to generate a diverse set of binding pockets. It varies in chain length from 14 to 18, and in molecular weight from 1000 to 5000. Then, the library was screened for sensitivity and selectivity towards SARS-CoV-2 nucleocapsid (N) and spike (S) proteins. The optimized nanosensor for each protein showed response times within 5.1 min and a detection LOD of 48 fM and 350 pM each. These nanosensors maintained identical performance for N protein even under human saliva conditions, which further validated their potential for on-site applications beyond the laboratory setting by integrating them into mobile benchtop systems. This showed the feasibility of simple diagnostic systems for widespread use on-site.

Pinals *et al.* also developed a SWCNT optical sensor for SARS-CoV-2 detection based on angiotensin-converting enzyme 2 (ACE2) functionalization, a host protein that exhibits strong binding capability to the S protein of SARS-CoV-2 and also with ssDNA (Fig. 2e).[35] $(GT)_6$ was selected due to its ability to yield a high suspension of SWCNTs and its propensity for the quicker and more extensive desorption of shorter ssDNA sequences in the presence of proteins. Unlike previous attempts with protein–SWCNT conjugate sensors that often used enzymes or protein, this new nanosensor employs human host cell membrane protein ACE2 to bind with the SARS-CoV-2 S protein receptor-binding domain (S RBD), enabling rapid and label-free protein detection. The nanosensor showed strong fluorescence enhancement to SARS-CoV-2 S protein within a 90 min timeframe achieving a LOD of 12.6 nM. The nanosensor was effectively passivated for S protein detection in saliva and viral transport medium. Additionally, the nanosensor demonstrated the capability of rapid detection of S protein and virus-like SARS-CoV-2 virions within seconds through real-time imaging by nIR fluorescence microscopy. With this high sensing performance, the nanosensor can be utilized in practical diagnosis if the sensor materials are well integrated with mobile form factors with optical instruments for on-site monitoring.

So far, we have utilized SWCNT nanosensors for diagnostics through multiple sensor arrays to various analytes. To further advance this, we can incorporate machine learning to identify intricacies that may be too subtle or complex for human eyes or current analytical methods to detect. The SWCNT nanosensor synthesis and screening process employs a heuristic approach, necessitating the individual synthesis of each nanosensor candidate prior to screening, which limits the expansion of

potential sensor libraries. To improve this bottleneck, research is increasingly leveraging machine learning to expedite sensor characterization and discovery.

Yaari *et al.* developed an ssDNA-SWCNT nanosensor complex to detect cancer biomarkers, especially HE4, CA-125, and YKL-40 (Fig. 2f). A total of 132 different DNA-SWCNT complexes were synthesized using eleven ssDNA sequences and 12 semiconducting SWCNT species. These nanosensors were then exposed to laboratory samples and cancer patient uterine lavage samples. Various machine learning models including support vector machine (SVM), random forest (RF), and artificial neural network (ANN) were employed to detect biomarkers. Among these, RF and ANN with a DNA sequence based feature vector were chosen due to better performance.[36]

For biofluid sensing in conjunction with machine learning, it is essential to have a variety of synthetic molecule candidates for specific analytes, and an experimental diversification evolution approach is also very important. Jeong *et al.* carried out a high throughput evolutionary study to identify serotonin, a key neurotransmitter associated with memory and learning, using a 6-mer (C)6 sequence known for its affinity to SWCNTs.[37] This library, containing over 69 billion unique sequences, facilitated the development of nanosensors that can be generalized for creating additional probes for neuromodulators.

Additionally, machine learning models can autonomously learn the correlation between DNA sequences that elicit strong unique responses in each sensor and the fluorescence response to analytes, thereby assisting and improving the selection of sensor candidates, which can aid in diagnostics.[38] Moreover, this machine learning based sensor technology offers distinct advantages for clinical uses. It has the potential to quickly adapt for detecting various diseases beyond ovarian cancer, addressing issues of biomarker selectivity in multi-analyte tests, facilitating high-throughput screening for large populations, and serving as a rapid and cost-effective screening tool without antibody.[39]

3. Hydrogel implantation of SWCNT sensors

For direct diagnosis within the body and to observe pathological kinetics in real-time, SWCNTs must be well interfaced with the target site of the living organisms. If direct injection of the materials is difficult due to penetration depth or chemical instability, SWCNTs should be embedded in a biocompatible substrate and implanted as a module. Hydrogels, 3D cross-linked porous hydrophilic polymer materials, have shown very attractive properties for this SWCNT implantation due to their mechanical flexibility, diffusion ability, controllable physicochemical properties, and excellent biocompatibility.[40,41] Furthermore, hydrogels can encapsulate various sizes of molecules with loading into their matrix through the porous structure, enabling selective penetration of the target analytes based on their specific sizes.[42,43] SWCNTs, especially, provide advantages for hydrogel implantation primarily due to their unique fluorescence properties in the nIR range (*e.g.* 800–1400 nm). The overall nIR spectrum encompasses 700–1700 nm and within the range, fluorophores are often divided into two sub-regions: nIR-I and nIR-II. Particularly, SWCNTs emit nIR-II range fluorescence, which possesses superior tissue penetration abilities. Reduced absorption and scattering by biological components, such as blood and proteins, in the nIR-II range allow light to penetrate deeper tissue regions, and enhance the contrast by non-overlapping with tissue autofluorescence.[44,45]

The early stage SWCNT hydrogel implantation was performed by Iverson *et al.* to detect nitric oxide (NO) as a biomarker to diagnose transient inflammation.[46] NO rapidly produces reactive oxygen/nitrogen species from reaction with the superoxide anion and following reactions. If these reactive species are overproduced in chronic inflammation, it can cause damage to all types of cellular biomolecules and even cancer.[47,48] For tissue-specific localization of the sensor and detection of NO *in vivo*, researchers implanted alginate-encapsulated $(AAAT)_7$-SWCNT sensors into the subcutaneous tissue of the flanks of mice. They successfully observed nIR fluorescence quenching associated with a burst of NO due to gel implantation through fast quenching and multiple-day fluorescence recovery, prolonged absence of NO and non-recruitment of macrophages, which are producers of NO. They also confirmed the long-term durability of the implanted hydrogel-SWCNT sensor. The gel remained intact for more than 400 days although the gel morphology slightly changed due to mice movement, and the fluorescence intensity was almost maintained with only a 14% decrease. The importance of monitoring inflammatory responses continues until recently, more large molecules such as the interleukin-6 (IL-6) family of cytokines have been detected using SWCNT nanosensors.[49,50]

Detection of pathogenic microorganisms such as bacteria is also pivotal for the early diagnosis of both acute and chronic infectious diseases. The timely identification facilitates rapid intervention restraining the progression of infections, and minimizing associated complications. Nißler *et al.* developed a nIR fluorescent SWCNT hydrogel nanosensor array and used that for remote fingerprint identification of clinically important six bacteria species including *S. aureus*, *S. epidermidis*, *S. pyogenes*, *E. faecalis*, *E. coli*, and *P. aeruginosa*.[51] In particular, by controlling the concentration of PEGDA, hydrogels with different porosities were used to match the target analyte size. They integrated one reference sensor, four generic lower-selectivity sensors, and four specific sensors targeting virulence factors including lipopolysaccharides, siderophores, DNases, and proteases. With a mixture of specific and non-specific sensors, background sensor responses in the final analysis were reduced or accounted for. They monitored the unique fluorescent fingerprint of six pathogens within 24 to 72 h and clustered different species using multivariate statistical analysis, a statistical method that reduces high-dimensional

data to low dimensions while preserving the variance of multivariate data as much as possible (Fig. 3a).[52] It is noteworthy that sensors were encoded even through below 7 mm thick tissue by using SWCNTs.

Researchers have also developed SWCNT hydrogels for monitoring of the treatment process, which is after the diagnosis step, such as the dosing and chemotherapeutic activity in real-time and *in vivo*. Through these studies, drug injection parameters such as drug administration time, amount, and frequency can be optimized to maximize treatment effectiveness and minimize harmful cytotoxicity with nanomaterial design devices.[53–56] Son *et al.* devised encapsulating ss$(GGGT)_3$-SWCNT SWCNT with PEG diacrylate hydrogel for selective detection of the chemotherapeutic temozolomide (TMZ) and its metabolite 5-aminoimidazole-4-carboxamide (AIC) to real-time monitor drug activity in SKH-1E mice and preserved fetal pig under *in vivo* conditions.[57] In particular, this research shows the possibility of better treatment for glioblastoma patients. The current treatment protocol for individuals with glioblastoma involves surgery to remove the tumor, followed by simultaneous radiation and chemotherapy using TMZ.[58] The SWCNT embedded hydrogel showed immediate utility of the device with real-time chemotherapeutic monitoring in the presence of U-87 MG human glioblastoma cells and as a subcutaneous implant in SKH-E1 mice, revealing the concentration, flux and local metabolic activity.[57] Upon injecting 100 μM TMZ into SKH-E1 mice, it was observed that the optical intensity of the sensor

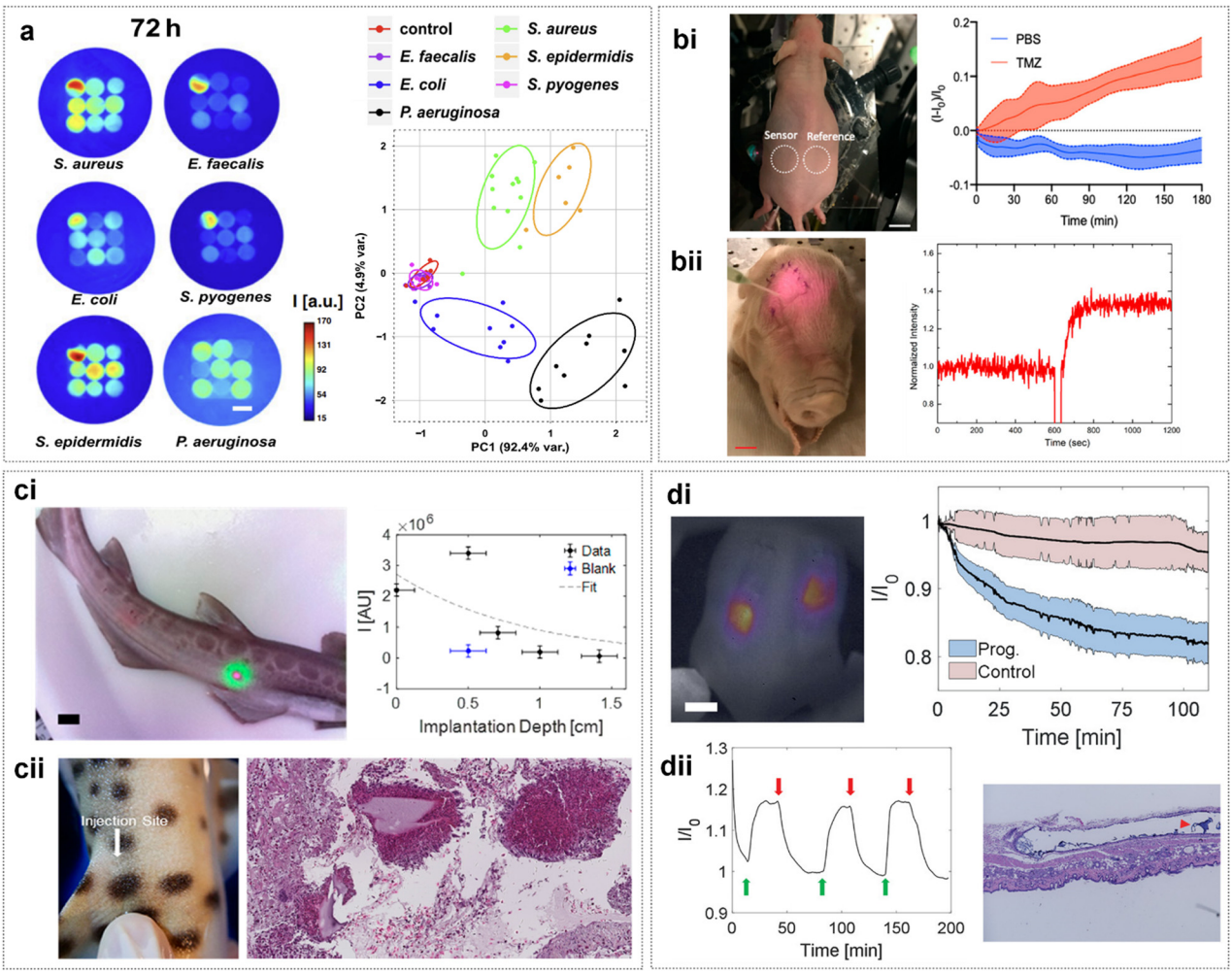

Fig. 3 Hydrogel implantation approach of SWCNT nanosensors for *in vivo* diagnostics and treatment. (a) Remote nIR fluorescent fingerprint of six pathogens and multivariate statistical analysis used to cluster different bacterial species. Reprinted with permission from ref. 51. Copyright 2020 Springer Nature. (bi) Real-time monitoring of TMZ in SKH-E1 mice and (bii) AIC molecules in preserved fatal pig by nanosensor integrated hydrogel implantation. Reprinted with permission from ref. 57. Copyright 2022 American Chemical Society. (ci) Optical penetration depth of ss$(AC)_{15}$-(6,5) SWCNT-hydrogel for detecting riboflavin in skin of catshark (*Galeus melastomus*). (cii) Implantation site in catshark (*Scyliorhinus stellaris*) and subcutaneous tissue surrounding the implant in turtle (*Pseudemys concinna*). Reprinted with permission from ref. 61. Copyright 2018 American Chemical Society. (di) *In vivo* progesterone monitoring with subcutaneous implanted p(AA54-ran-S_{22}-ran-AC4)-(7,6) SWCNT hydrogel inside of dialysis bags in SKH1-E mice. (dii) Stable and reversible sensor response under alternating cycles and well-healed tissue imaging after hydrogel implantation. Reprinted with permission from ref. 68. Copyright 2020 John Wiley & Sons.

hydrogel increased over time due to the degradation of TMZ to AIC within the body (Fig. 3bi). Moreover, utilizing the recently developed wavelength-induced frequency filtering (WIFF) technique, the sensor can be utilized even when positioned 2.1 cm beneath the cranium within intact porcine brain tissue, indicating the significant potential of SWCNTs for deep-tissue *in vivo* monitoring (Fig. 3bii).[59]

The SWCNT embedded hydrogel can be also well interfaced on marine organisms characterized by wet and rough skin and dynamic activity. Lee *et al.* specifically aimed for the monitoring of riboflavin levels in nine species of aquatic vertebrates. Riboflavin serves as a precursor for both flavin mononucleotide (FMN) and flavin adenine dinucleotide (FAD) which are two important coenzymes in oxidative phosphorylation.[60] Oxidative phosphorylation is the main metabolic pathway of energy production in mitochondria, converting ADP into ATP. Researchers fabricated sensors by encapsulating ss$(AC)_{15}$-(6,5) SWCNTs into a biocompatible poly(ethylene glycol) diacrylate (PEGDA) hydrogel for *in vivo* riboflavin sensing.[61] After hydrogel implantation, the behaviour patterns in species such as eel, catshark, turtle, and goldfish exhibited neither impairment nor erratic patterns, which is indicative of high tolerance to implants. Moreover, they confirmed the optical penetration depth in teleosts and catsharks. The SWCNT-hydrogel implants were discerned up to a depth of 7 mm, showing a distinct contrast when compared to a nonfluorescent hydrogel implanted at a depth of 5 mm (Fig. 3ci). Notably, the implantation site in the catshark was observed to have fully healed by 33 days post-implantation. In particular, in the ultrasound images captured 4 weeks after implantation, the implantation site was identified *via* a slight change in tissue structure and echogenicity, but the surrounding tissue was completely normal (Fig. 3cii). For significant foreign body reactions, larger changes in architecture and echogenicity will be found in the periphery of the implant as it becomes encapsulated.[62,63] This research suggests the potential of SWCNT hydrogels for marine biologging and inspires the development of wearable and optoelectronic sensor tags using them.

Recently, much research has been conducted to detect steroids, which regulate various important functions of the human body and cause various diseases if dysfunctional.[64–67] Lee *et al.* used polymer-SWCNT sensors to detect 11 physiologically and therapeutically significant human steroids, including cortisol and progesterone.[68] In particular, progesterone determines female sexual traits such as differentiation, menstruation, and pregnancy.[69] Its dysregulation causes female diseases such as breast cancer or endometriosis.[70,71] They overcome the limitation of relying on the generated library by functionalizing SWCNTs with self-templating polymers. Acrylated cortisol appendages ware attached to the polymer backbone composed of hydrophobic styrene monomers and alkyl chains, and hydrophilic acrylic acid monomers and carboxylic acid groups. They implanted a 6–8 Koda dialysis bag containing PEGDA hydrogel encapsulating the optimized progesterone-targeting sensor subcutaneously into mice, and monitored changes under an *in vivo* environment (Fig. 3di). The reason for using the dialysis bag is that sensitivity and sustainability are improved compared to not using it. Subsequent sensor response under alternating cycles and implanted tissue images support the stability, reversibility, and biocompatibility of the hydrogel sensor (Fig. 3dii).

Even though significant advances have been achieved with versatile hydrogel implantation techniques of SWCNTs, several challenges remain to be overcome for human biomedical purposes of SWCNTs. The efficiency of encapsulating hydrophobic nanoparticles in the hydrophilic porous network of hydrogels is still low.[72] In addition, the weak mechanical properties of hydrogel layers make them prone to tearing and deforming during animal movements.[73] There is also the possibility of undesired degradation or clearance from the implantation sites due to the immune reaction from host organisms.[74] If these additional detailed technical points are addressed, SWCNT-hydrogel implantation could become a leading candidate for stable and selective real-time diagnostics.

4. Direct injection of SWCNTs into organisms

Hydrogel based implantation is a very powerful tool for *in vivo* diagnostics using SWCNTs, however, for organisms having thinner tissues than animals including as plants or insects, it is challenging to insert relatively thick materials such as hydrogel. In addition, when there is a need to diagnose following the flow of biofluid inside the animals or to image only specific precise areas, a direct and precise injection would be more efficient too. Thus, direct injection of SWCNT materials would be another powerful interfacing technique for real-time diagnosis. Injected SWCNTs can immediately interact with the analyte wave after injection, which should result in faster and more accurate real-time responses. With appropriate surface functionalization compatible with cells or tissues, direct injection of SWCNTs can pave the way to real-time diagnostics and monitoring for humans, animals, and even plants, heralding a transformative paradigm in *in vivo* medical assessments.

One critical infectious disease is endocarditis, a swift and destructive infection of the heart valves. Infective endocarditis is notorious with high mortality rates of ~15–47%, and *S. aureus* is the most common infective pathogen related to it.[75,76] Bardhan *et al.* innovatively harnessed SWCNTs as a probe for non-invasive fluorescence imaging of *S. aureus* Xen-29 by functionalizing SWCNTs with M13 bacteriophage (M13-SWCNT).[77] The probe was enhanced by conjugating an anti-bacterial antibody to M13-SWCNT, refining its specificity towards certain F′-negative bacterial strains. This complex was subsequently injected intravenously into mice, localized in the right thigh muscle at the site of infection, and proved capable of detecting infectious bacteria with fluorescent imaging.

Metabolic diseases or disorders profoundly impact human health because the processes are associated with basic biochemical reactions intrinsic to our physiology. One of the

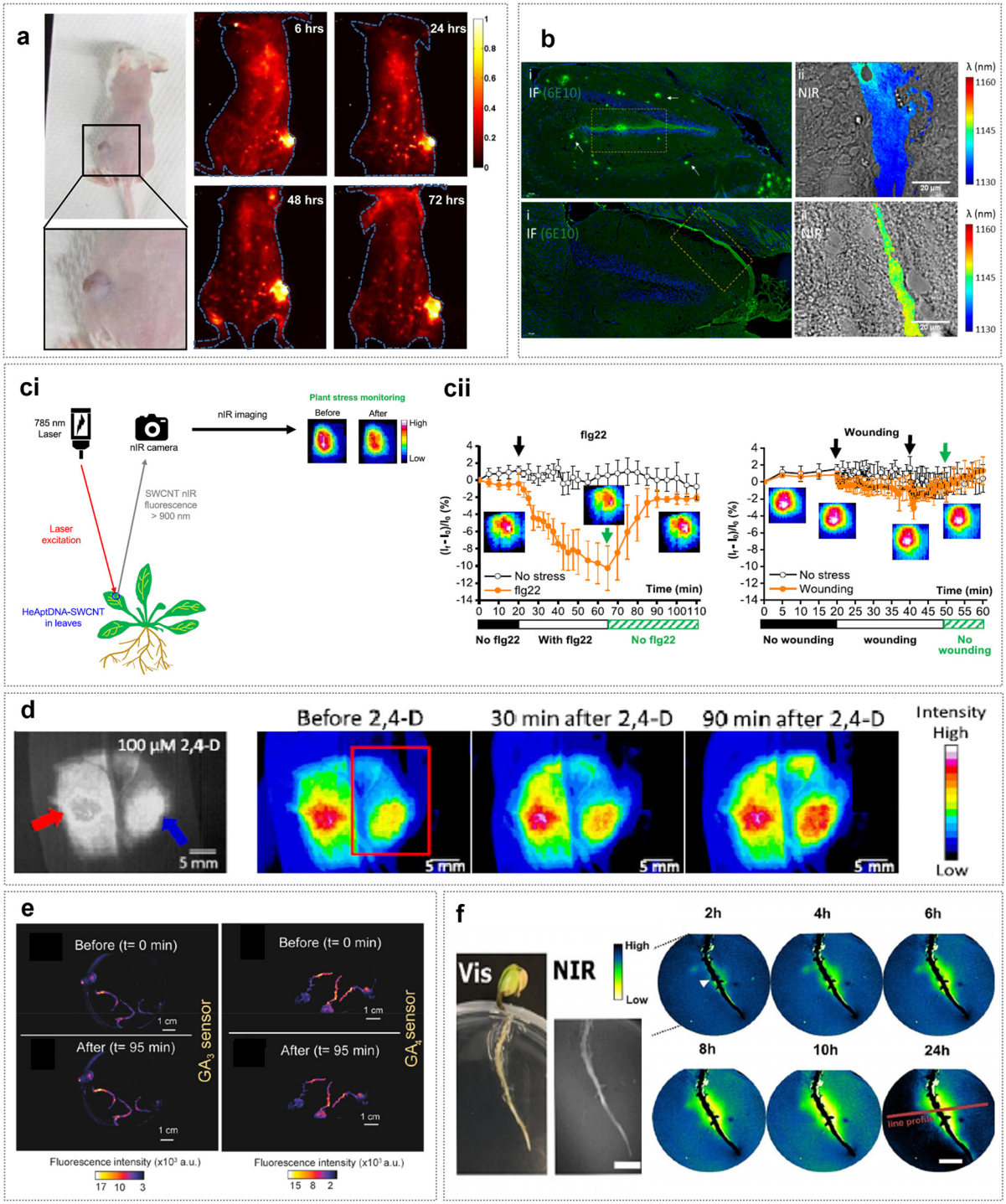

Fig. 4 Direct injection approach of SWCNT nanosensors for *in vivo* diagnostics. (a) *In vivo* imaging of xenograft 4T1 tumor in a murine model with high uptake of C_{18}-PMH-mPEG-SWCNT. Reprinted with permission from ref. 84. Copyright 2012 American Chemical Society. (b) ABCNT for detecting Aβ intracranially *in vivo* to early diagnose Alzheimer. Immunolabeled hippocampal section (bottom-left) and nIR hyperspectral map of ABCNT emission wavelength derived from the yellow highlight box (bottom-right). Reprinted with permission from ref. 86. Copyright 2022 American Chemical Society. (ci) HeAptDNA-SWCNT sensors quench the fluorescence intensity with the response of H_2O_2. (cii) *In vivo* monitoring of the conditions of flg22 and wounding. Reprinted with permission from ref. 97. Copyright 2020 American Chemical Society. (d) *In vivo* spatiotemporal imaging for 2,4-D with PF(1,3-P)HCl conjugated SWCNTs in spinach leaves. Reprinted with permission from ref. 98. Copyright 2021 American Chemical Society. (e) Photoluminescence response of the GA-SWCNT sensor after GA_3 and GA_4 were added. Reprinted with permission from ref. 99. Copyright 2023 American Chemical Society. (f) Monitoring with PEG-lipids-SWCNT for pathogen-induced polyphenol release from plant roots. Reprinted with permission from ref. 100. Copyright 2021 John Wiley & Sons.

major reasons causing metabolic disorders is lipid accumulation in hepatic cells and tissues, implicated in diverse pathologies including lysosomal storage disorders, atherosclerosis, non-alcoholic fatty liver disease (NAFLD), and drug-induced phospholipidosis (DIPI).[78–80] Galassi *et al.* detected hepatic lipid accumulation in animal models of the lysosomal lipid storage diseases, Niemann–Pick disease type A/B (NPA/B) and Niemann–Pick disease type C (NPC).[81] They used a SWCNT nanosensor to real-time monitor the accumulation of lipids in Kupffer cells (KCs) of endolysosomal organelles and the effects of dietary intervention in mouse models of NAFLD and non-alcoholic steatohepatitis (NASH). The nanosensor consists of (9,4) SWCNTs non-covalently conjugated with the single stranded oligonucleotide CTTC3TTC, allowing SWCNTs to be well documented in the cells or tissues similar to the process of PEG ligation. When injected intravenously, the nanosensor was specifically localized within KCs, and showed fluorescence changes due to injection of oxidized low-density lipoprotein.

SWCNT nanosensors have been also applied for *in vivo* fluorescence imaging of tumor with direct injection. SWCNTs can detect significant tumor accumulation due to the enhanced permeability and retention (EPR) effect, even in the absence of specific targeting agents.[82,83] For *in vivo* tumor imaging, Robinson *et al.* injected long circulating functionalized SWCNTs intravenously into a mouse with subcutaneous xenograft 4T1 tumors located on the right hind limb.[84] They coated SWCNTs non-covalently with relatively large 90 kDa amphiphilic poly(maleic anhydride-alt-1-octadecene) – methoxy-poly(ethylene glycol) (C_{18}-PMH-mPEG). Video-rate fluorescence images based on the nIR fluorescence of SWCNTs were taken continuously immediately after nanosensor injection to track SWCNTs moving through the blood circulation in real time for up to 210 s. Due to extended circulation of SWCNTs and their ongoing accumulation in tumor spaces because of the EPR effect, there was a consistent rise in nIR fluorescence in the tumor areas in all the tested mice, persisting for 72 hours (Fig. 4a). Furthermore, this research suggests the possibility that further optimization, such as attaching targeting agents to SWCNTs, could enhance tumor uptake.[85]

As the incidence of degenerative neurological diseases rises due to the increase in the elderly population, accurate initial diagnosis and appropriate care intervention are becoming more important. The most representative degenerative neurological disease is dementia. Antman-Passig *et al.* recently engineered an innovative nIR SWCNT-sensor to detect amyloid-beta (Aβ) intracranially *in vivo*, a biomarker of the early stages of Alzheimer's disease (AD).[86] The asymptomatic phase of AD is marked by undetectable structural and molecular abnormalities in the brain, which include the accumulation of Aβ, formation of tau tangles, and neurodegeneration.[87–89] The Aβ-functionalized carbon nanotubes (ABCNTs) selectively respond to Aβ *via* solvatochromic modulation in the nIR emission of the nanotube.[86] The emission spectra of ABCNTs intracranially injected into 8-month-old 5XFAD and WT mice showed a significant blue-shifted effect only in 5XFAD mice. The researchers also confirmed a localized pool of ABCNTs in the hippocampus region using nIR hyperspectral microscopy. Since the nIR hyperspectral system collects the fluorescence spectra in each point of the field of view, it provides both spatial and spectral information simultaneously. Thus, it can diagram the distribution of photoluminescent responses from *in vivo* interfaces.[90] The immunolabeled hippocampal section showed high load of Aβ aggregates in 8-month-old 5XFAD mice (Fig. 4b). By spectrally resolving the region of ABCNTs, they found a broad distribution of nanotube emission wavelengths in the 5XFAD mice compared to WT, and overall blue-shifted (9,4) center wavelength (Fig. 4b). This research provides insights from deep tissue sections (2 mm) and offers a technology that allows the exploration of molecular pathways associated with Aβ neurotoxicity during the progression of AD in living organisms.

When a SWCNT sensor is directly injected into plants, we can monitor their defence mechanisms triggered by various factors that cause stress and find things necessary for their growth.[91,92] In addition, we can check the soil conditions about the presence of pathogens, salinity, or drought and atmosphere in terms of air pollutants by injecting nanosensors into plants.[93,94] This is important as global population growth has increased the demand for food production, but food production is not keeping up with the demand.[95,96]

Hydrogen peroxide (H_2O_2), one of the reactive oxygen species (ROS), is a signalling molecule used in cell-to-cell communication to enhance and revitalize the defence mechanisms of plants. However, ROS diffuse very fast with short lifetime due to their high activity, making it hard for them to be detected with a sensor. Wu *et al.* designed a DNA aptamer based SWCNT sensor that binds with porphyrin hemin (HeAptDNA-SWCNT).[97] They gently pressed the tip of a syringe to infiltrate the SWCNT nanosensor solution into the lower side leaves of *Arabidopsis thaliana* plants, then confirmed the quenching of SWCNTs caused by H_2O_2 using nIR optical imaging (Fig. 4ci). SWCNT nIR quenching occurs when plants are stressed by UV-B stress, intensive light, and pathogens such as flg22, but in contrast, there is no significant change with leaf wounding (Fig. 4cii). The biocompatibility of the SWCNT sensor in plant was demonstrated by the high similarity in differences in the percentage of dead cells and plant photosynthetic performance before and after injection.

Synthetic auxins including 1-naphthalene acetic acid (NAA) and 2,4-dichlorophenoxyacetic acid (2,4-D) are used as plant growth hormones. Rapid detection of these compounds in plants will improve our knowledge relating hormone distribution and allow for their more efficient use. Ang *et al.* chose 6 cationic polymers for wrapping SWCNTs to enable electrostatic interactions with anionic plant hormone analytes, and detect 13 analytes including natural auxins, synthetic auxins, cytokines, and other plant hormones.[98] The

SWCNT sensor was infiltrated into spinach leaves through the mid-leaf vein, followed by analyte infiltrations. According to *in vivo* monitoring of spatiotemporal distribution, four analytes namely 3-indole propionic acid (IPA), 3-indole butyric acid (IBA), NAA, and 2,4-D respond noticeably to each sensor (Fig. 4d). The sensor targeting 2,4-D showed 51% turn on response and the sensor targeting NAA exhibited 50% quenching response.

Soil conditions can sometimes stress plants, triggering the secretion of plant hormones. Therefore, it is meaningful to measure the level of gibberellin (GA) in plant roots, but the molecular structures of various GAs are similar, making it difficult to distinguish between them. Boonyaves *et al.* selected 11 polymers with styrene derivative monomers, such as sodium-styrenesulfonate or vinyl benzyl trimethylammonium chloride, for SWCNT functionalization to induce hydrogen bonding with GAs which have carboxyl groups.[99] As a result, it was possible to distinguish between GA_3 and GA_4 using the polymers of S-gluAPM and N-gluAPM. Even after injecting the sensors into basil roots, the performance was maintained, and fluorescence response due to GA_3 and GA_4 could be confirmed through nIR imaging (Fig. 4e). These sensors were finally used at high soil salinity to monitor the effect of salinity on the decrease of fluorescence intensity.

Plants use polyphenols secreted from leaves and roots to protect themselves from pathogens and herbivores. Therefore, when polyphenols are detected, plant stress caused by pathogens can be numerically confirmed. Nissler *et al.* found that various structures of polyphenols could be detected if the SWCNT surface was non-covalently modified using ssDNA and PEG-lipid macromolecules with different surface chemistries and different nucleotide compositions.[100] The rationale behind this approach is that compounds such as tannins have multiple hydroxy groups and can influence SWCNT sensors to form strong interaction with polyphenols. To inject the SWCNT sensors into plants, these sensors were embedded in culture medium agar and soybean seedlings were grown on it. The researchers caused embryonic roots to release polyphenols with a stimulus of pathogen-derived elicitor, a branched β-glucan cell wall component of the oomycete fungus *Phytophthora sojae*, and monitored the intensity change of sensors (Fig. 4f).

Direct injection of SWCNTs into living organisms presents a complex challenge that must meet biocompatibility requirements beyond their utilization as imaging agents or passive delivery systems. Despite extensive research, comparing biocompatibility results remains difficult due to variations in the materials, surface chemistry, and biological context being evaluated.[101] It is essential that SWCNT nanosensors not only avoid adverse biological interactions but also demonstrate sustainability within biological systems over long periods of time *in vivo*. Oxidative degradation of SWCNTs by immune cells such as neutrophils and macrophages is an important consideration in this regard.[102–104] Researchers suggest that the path to mitigating unexpected side effects and achieving long-term stability in sensor applications may depend on the development of stable biocompatible functionalization strategies.[105–107] This requires efforts to consider both achieving sensitivity to specific target analytes through functionalization and maintaining biocompatibility and robustness in a dynamic *in vivo* environment.

5. Conclusions and outlook

We have reviewed the technological advances in the use of nIR fluorescence of SWCNTs for versatile diagnostics. SWCNTs with their distinct structure-dependent nIR emission have shown significant potential for broad-spectrum diagnostics. A wide range of polymers, DNA, organic molecules, or small molecules for SWCNT functionalization are highly desirable as they not only ensure the reliable dispersion of SWCNT sensor materials in aqueous solutions but also act as synthetic, non-biological counterparts to antibodies. This enables them to selectively identify and bind to specific target molecules. The advent of advanced recognition techniques including CoPhMoRe amplifies this potential, paving the way for the development of biosensors of unparalleled efficacy rooted in diagnostics. By synergizing these recognition elements with SWCNTs, it becomes feasible to discern various analytes with remarkable specificity and sensitivity.

SWCNTs have demonstrated their broad-spectrum diagnostic efficiency not just under controlled laboratory conditions but also in real-world applications. Tailored interfacing methods of SWCNTs including direct biofluid sensing, hydrogel implantation and direct injection have demonstrated the transformative potential of SWCNTs as optical diagnostic tools. We summarized and compared the detailed sensing performances of SWCNTs with their target analytes and diseases (Table 1). Their adaptability and efficacy across these diverse domains accentuate their robustness and underpin their continued significance in future diagnostic endeavors. We hope that the readers can predict the performance range that will be achieved by combining SWCNTs with a certain construct in advance based on this information. The versatility of SWCNTs is evident, and their potential in diagnostic sensor applications across various sectors is immense and still burgeoning.

However, many challenging issues still remain with the use of SWCNTs for real-world diagnostics and treatment of patients. First, diagnostic criteria must be established for SWCNTs based on accurate statistics from a vast number of tests on actual clinical samples. To ensure the efficacy of SWCNT-based diagnostics, it is crucial to establish criteria for sensitivity and specificity, set quantification limits for biomarker detection, and guarantee reproducibility and reliability across various testing conditions. Criteria for biocompatibility and safety are vital to prevent adverse patient reactions, while calibration standards and sample handling protocols are essential for maintaining diagnostic accuracy.[108] The success of SWCNT-based diagnostics depends on comprehensive clinical validation that confirms their effectiveness and reliability in diverse patient populations. In addition, it is prerequisite to have

Table 1 Sensor constructs and performances of nIR fluorescent SWCNTs for broad-spectrum diagnostics

Diagnosis methods	Diagnosed disorder	Biomarkers	SWCNT construct	Limit of detection (LOD)	Detection range	Ref.
Direct biofluid sensing	Microalbuminuria	Albumin	Carboxylate-poly-carbodiimide polymers-SWCNT	3 mg L^{-1}	1.56 to 100 mg L^{-1}	26
	Blood coagulation	Fibrinogen Thrombin	DPPE–PEG-SWCNT	0.012 mg mL^{-1}	5×10^{-4} to 0.5 mg mL^{-1}	27
	Diabetes	Insulin	PEGylated lipids-SWCNT	N.A	180 pM to 3.5 μM	31
	Diabetes	Insulin	C_{16}-PEG (2000 Da)-ceramide SWCNT $(AT)_{15}$-Insulin aptamer-SWCNT	1.3×10^{-5} mg mL^{-1}	3.3×10^{-6} to 0.3 mg mL^{-1}	33
	COVID-19	SARS-CoV-2 N, S protein	PEG-lipid-SWCNT	48 fM 350 pM	1 fM to 10^2 nM	34
	COVID-19	SARS-CoV-2 S protein receptor-binding domain	ACE2-$(GT)_6$-SWCNT	12.6 nM	10^{-3} to 10^3 nM	35
	Gyneclogic cancer	HE4 CA-125 YKL-40	Combination of 12 SWCNT species and 11 DNA sequences	N.A	N.A	36
Hydrogel implantation	Inflammatory disease	Nitric oxide	PEG-$(AAAT)_7$-PEG $(AAAT)_7$-PEG in alginate hydrogel	1 μM N.A	N.A N.A	46
	Infectious diseases	Lipopolysaccharides	$(GT)_{20}$-ssDNA-linker-LPS-binding peptide in high porosity PEGDA hydrogel	12.5 μM	0.2 to 50 μM	51
		Siderophores	Hemin-aptamer-SWCNT in low porosity hydrogel	10 μM	0.08 to 50 μM	
		DNases	Genomic, denatured calf thymus (CT) ssDNA-SWCNT in high porosity PEGDA hydrogel	N.A	11 UN mL^{-1} to 55 μg mL^{-1}	
		Proteases	BSA-SWCNT in high porosity PEGDA hydrogel	N.A	13.5 U mL^{-1} to 18 μg mL^{-1}	
	Glioblastoma	Temozolomide	ss$(GGGT)_3$-SWCNT	TMZ: 30 μM AIC: 14 μM	10^{-9} to 10^{-3} M	57
		5-Aminoimidazole-4-carboxamide	ss$(GGGT)_3$-SWCNT in PEG diacrylate hydrogel	N.A	>2.1 cm brain tissue and skull	
	Oxidative phosphorylation	Riboflavin	ss$(AC)_{15}$-(6,5) SWCNT in PEGDA hydrogel	>7 mm skin and muscle tissue	N.A	61
	Female cancers	Progesterone	p(AA_{54}-ran-S_{22}-ran-AC_4)-(7,6) SWCNT in PEGDA hydrogel in dialysis bag	N.A	100×10^{-6} M under subcutaneous implantation	68
Direct nanosensors injection	Endocarditis	*Staphylococcus aureus*	M13-SWCNT	N.A	N.A	77
	Niemann–Pick disease, NAFLD, NASH	Endolysosomal lipid	ssCTTC_3TTC-SWCNT	N.A	2 to 200 μM	81
	4T1 murine breast cancer	Xenograft 4T1 tumor	C_{18}-PMH-mPEG-SWCNT	N.A	N.A	84
	Alzheimer's disease	Amyloid-beta	Sodium deoxycholate-amyloid-beta-SWCNT	100 nM in PBS 1 μM in 33% serum	10^{-1} to 10^3 nM	86
	Plant stress	Hydrogen peroxide	HeAptDNA-SWCNT	N.A	1 to 1000 μM	97
	Plant growth	Synthetic auxins-NAA Synthetic auxins-2,4-D	Cationic poly(*N*-vinyl imidazolium)-SWCNT, cationic fluorene-co-phenyl polymer-SWCNT	8.2 μM 0.35 μM	10^{-1} to 10^3 μM	98
	Soil salinity	$Gibberellin_3$ $Gibberellin_4$	S-gluAPM-SWCNT N-gluAPM-SWCNT	N.A N.A	N.A N.A	99
	Stress of plant from pathogens	Tannic acid Genistein	ssDNA-SWCNT PEG-lipid-SWCNT	N.A N.A	10^{-9} to 10^{-3} M 10^{-8} to 10^{-4} M	100

synthesis and processing technology that can mass-produce a specific SWCNT construct with consistent sensing performance and physical specifications. We will also need to develop hardware technology that can consistently combine mass-

produced SWCNT sensor materials with user-friendly analytic form-factors. Lastly, it is ultimately necessary to develop software that can accurately calculate signals measured from hardware combined with such consistent sensor materials at high speed. Addressing this, the development of deep learning-driven methodologies for noise and signal discrimination, coupled with advanced image analysis techniques, becomes crucial. Such tasks will require much more effort moving forward.

Given the diversity and presence of active reference analytes in various biofluids, future research should explore methods to enhance the intrinsic selectivity and signal stability of SWCNTs for diagnostics in complex environments. Furthermore, as diagnostic applications shift towards the use of hydrogel integration and nanosensor injections, there is a big need to address the challenges posed by mechanical noise, which can significantly reduce the signal-to-noise ratio (S/N).

Since the field has already successfully undertaken the challenging tasks of elucidating the physical properties of these very small materials, we believe that the integration of production processes, hardware, and software will proceed much more smoothly in near future, and we can truly achieve accurate and rapid smart diagnostics using these novel materials.

Author contributions

Minyeong Yoon: writing – original draft. Yullim Lee: writing – original draft. Seungju Lee: writing – review & editing. Youngwook Cho: review & editing. Damee Koh: review & editing. Seyoung Shin: review & editing. Youngho Song: review & editing, Changyu Tian: review & editing, Joohoon Kang: review & editing, Soo-Yeon Cho: writing – original draft, supervision, funding, resources, project administration.

Conflicts of interest

There are no conflicts to declare.

Acknowledgements

This research was supported by the National Research Foundation (NRF) grant funded by the Korean government (MSIT) (No. RS-2023-00211580, RS-2023-00237308).

References

1 G. Hong, S. Diao, A. L. Antaris and H. Dai, *Chem. Rev.*, 2015, **115**, 10816–10906.
2 J. H. Heo, M. Sung, T. Q. Trung, Y. Lee, D. H. Jung, H. Kim, S. Kaushal, N. E. Lee, J. W. Kim, J. H. Lee and S. Y. Cho, *EcoMat*, 2023, **5**(5), e12332.
3 S. Kruss, A. J. Hilmer, J. Zhang, N. F. Reuel, B. Mu and M. S. Strano, *Adv. Drug Delivery Rev.*, 2013, **65**, 1933–1950.
4 F. Wang, G. Dukovic, L. E. Brus and T. F. Heinz, *Science*, 2005, **308**, 838–841.
5 S. M. Bachilo, M. S. Strano, C. Kittrell, R. H. Hauge, R. E. Smalley and R. B. Weisman, *Science*, 2002, **298**, 2361–2366.
6 A. A. Boghossian, J. Zhang, P. W. Barone, N. F. Reuel, J. H. Kim, D. A. Heller, J. H. Ahn, A. J. Hilmer, A. Rwei, J. R. Arkalgud, C. T. Zhang and M. S. Strano, *ChemSusChem*, 2011, **4**, 848–863.
7 M. J. O'connell, S. M. Bachilo, C. B. Huffman, V. C. Moore, M. S. Strano, E. H. Haroz, K. L. Rialon, P. J. Boul, W. H. Noon and C. Kittrell, *Science*, 2002, **297**, 593–596.
8 C. Manzoni, A. Gambetta, E. Menna, M. Meneghetti, G. Lanzani and G. Cerullo, *Phys. Rev. Lett.*, 2005, **94**, 207401.
9 J. Pan, F. Li and J. H. Choi, *J. Mater. Chem. B*, 2017, **5**, 6511–6522.
10 S. Diao, G. Hong, J. T. Robinson, L. Jiao, A. L. Antaris, J. Z. Wu, C. L. Choi and H. Dai, *J. Am. Chem. Soc.*, 2012, **134**, 16971–16974.
11 C. Li, G. Chen, Y. Zhang, F. Wu and Q. Wang, *J. Am. Chem. Soc.*, 2020, **142**, 14789–14804.
12 J. Zhang, M. P. Landry, P. W. Barone, J. H. Kim, S. Lin, Z. W. Ulissi, D. Lin, B. Mu, A. A. Boghossian, A. J. Hilmer, A. Rwei, A. C. Hinckley, S. Kruss, M. A. Shandell, N. Nair, S. Blake, F. Sen, S. Sen, R. G. Croy, D. Li, K. Yum, J. H. Ahn, H. Jin, D. A. Heller, J. M. Essigmann, D. Blankschtein and M. S. Strano, *Nat. Nanotechnol.*, 2013, **8**, 959–968.
13 D. A. Heller, G. W. Pratt, J. Zhang, N. Nair, A. J. Hansborough, A. A. Boghossian, N. F. Reuel, P. W. Barone and M. S. Strano, *Proc. Natl. Acad. Sci. U. S. A.*, 2011, **108**, 8544–8549.
14 F. A. Mann, P. Galonska, N. Herrmann and S. Kruss, *Nat. Protoc.*, 2022, **17**, 727–747.
15 M. Kim, C. Chen, Z. Yaari, R. Frederiksen, E. Randall, J. Wollowitz, C. Cupo, X. Wu, J. Shah, D. Worroll, R. E. Lagenbacher, D. Goerzen, Y.-M. Li, H. An, Y. Wang and D. A. Heller, *Nat. Chem. Biol.*, 2023, **19**, 1448–1457.
16 T. Shiraki, H. Onitsuka, T. Shiraishi and N. Nakashima, *Chem. Commun.*, 2016, **52**, 12972–12975.
17 R. M. Williams, C. Lee, T. V. Galassi, J. D. Harvey, R. Leicher, M. Sirenko, M. A. Dorso, J. Shah, N. Olvera and F. Dao, *Sci. Adv.*, 2018, **4**, eaaq1090.
18 J. D. Harvey, P. V. Jena, H. A. Baker, G. H. Zerze, R. M. Williams, T. V. Galassi, D. Roxbury, J. Mittal and D. A. Heller, *Nat. Biomed. Eng.*, 2017, **1**, 0041.
19 D. Kozawa, S. Y. Cho, X. Gong, F. T. Nguyen, X. Jin, M. A. Lee, H. Lee, A. Zeng, G. Xue, J. Schacherl, S. Gibson, L. Vega and M. S. Strano, *ACS Nano*, 2020, **14**, 10141–10152.
20 S. Y. Cho, X. Gong, V. B. Koman, M. Kuehne, S. J. Moon, M. Son, T. T. S. Lew, P. Gordiichuk, X. Jin, H. D. Sikes and M. S. Strano, *Nat. Commun.*, 2021, **12**, 3079.
21 S. Y. Cho, V. B. Koman, X. Gong, S. J. Moon, P. Gordiichuk and M. S. Strano, *ACS Nano*, 2021, **15**, 13683–13691.
22 W. J. Peveler, M. Yazdani and V. M. Rotello, *ACS Sens.*, 2016, **1**, 1282–1285.
23 J. L. Gross, M. J. De Azevedo, S. P. Silveiro, L. H. Canani, M. L. Caramori and T. Zelmanovitz, *Diabetes Care*, 2005, **28**, 164–176.
24 J. L. Rodicio, C. Campo and L. M. Ruilope, *Kidney Int.*, 1998, **54**, S51–S54.

25 L. Jørgensen, I. Heuch, T. Jenssen and B. K. Jacobsen, *J. Am. Soc. Nephrol.*, 2008, **19**, 992.
26 J. Budhathoki-Uprety, J. Shah, J. A. Korsen, A. E. Wayne, T. V. Galassi, J. R. Cohen, J. D. Harvey, P. V. Jena, L. V. Ramanathan and E. A. Jaimes, *Nat. Commun.*, 2019, **10**, 3605.
27 E. Gerstman, A. Hendler-Neumark, V. Wulf and G. Bisker, *ACS Appl. Mater. Interfaces*, 2023, **15**, 21866–21876.
28 G. Bisker, J. Dong, H. D. Park, N. M. Iverson, J. Ahn, J. T. Nelson, M. P. Landry, S. Kruss and M. S. Strano, *Nat. Commun.*, 2016, **7**, 10241.
29 G. Wilcox, *Clin. Biochem. Rev.*, 2005, **26**, 19.
30 J. Almaça, A. Caicedo and L. Landsman, *Diabetologia*, 2020, **63**, 2076–2085.
31 G. Bisker, N. A. Bakh, M. A. Lee, J. Ahn, M. Park, E. B. O'Connell, N. M. Iverson and M. S. Strano, *ACS Sens.*, 2018, **3**, 367–377.
32 G. Grassi, P. Scuntero, R. Trepiccioni, F. Marubbi and K. Strauss, *J. Clin. Transl. Endocrinol.*, 2014, **1**, 145–150.
33 R. Ehrlich, A. Hendler-Neumark, V. Wulf, D. Amir and G. Bisker, *Small*, 2021, **17**, e2101660.
34 S. Y. Cho, X. Jin, X. Gong, S. Yang, J. Cui and M. S. Strano, *Anal. Chem.*, 2021, **93**, 14685–14693.
35 R. L. Pinals, F. Ledesma, D. Yang, N. Navarro, S. Jeong, J. E. Pak, L. Kuo, Y. C. Chuang, Y. W. Cheng, H. Y. Sun and M. P. Landry, *Nano Lett.*, 2021, **21**, 2272–2280.
36 Z. Yaari, Y. Yang, E. Apfelbaum, C. Cupo, A. H. Settle, Q. Cullen, W. Cai, K. L. Roche, D. A. Levine and M. Fleisher, *Sci. Adv.*, 2021, **7**, eabj0852.
37 S. Jeong, D. Yang, A. G. Beyene, J. T. Del Bonis-O'Donnell, A. M. Gest, N. Navarro, X. Sun and M. P. Landry, *Sci. Adv.*, 2019, **5**, eaay3771.
38 P. Kelich, S. Jeong, N. Navarro, J. Adams, X. Sun, H. Zhao, M. P. Landry and L. Vuković, *ACS Nano*, 2022, **16**, 736–745.
39 M. Kim, C. Chen, P. Wang, J. J. Mulvey, Y. Yang, C. Wun, M. Antman-Passig, H.-B. Luo, S. Cho, K. Long-Roche, L. V. Ramanathan, A. Jagota, M. Zheng, Y. Wang and D. A. Heller, *Nat. Biomed. Eng.*, 2022, **6**, 267–275.
40 A. Barhoum, O. Sadak, I. A. Ramirez and N. Iverson, *Adv. Colloid Interface Sci.*, 2023, 102920.
41 K.-H. Shen, C.-H. Lu, C.-Y. Kuo, B.-Y. Li and Y.-C. Yeh, *J. Mater. Chem. B*, 2021, **9**, 7100–7116.
42 Z. Li, X. Shan, Z. Chen, N. Gao, W. Zeng, X. Zeng and L. Mei, *Adv. Sci.*, 2021, **8**, 2002589.
43 R. Narayanaswamy and V. P. Torchilin, *Molecules*, 2019, **24**, 603.
44 K. Welsher, S. P. Sherlock and H. Dai, *Proc. Natl. Acad. Sci. U. S. A.*, 2011, **108**, 8943–8948.
45 G. Hong, J. C. Lee, J. T. Robinson, U. Raaz, L. Xie, N. F. Huang, J. P. Cooke and H. Dai, *Nat. Med.*, 2012, **18**, 1841–1846.
46 N. M. Iverson, P. W. Barone, M. Shandell, L. J. Trudel, S. Sen, F. Sen, V. Ivanov, E. Atolia, E. Farias, T. P. McNicholas, N. Reuel, N. M. Parry, G. N. Wogan and M. S. Strano, *Nat. Nanotechnol.*, 2013, **8**, 873–880.
47 P. C. Dedon and S. R. Tannenbaum, *Arch. Biochem. Biophys.*, 2004, **423**, 12–22.
48 L. M. Coussens and Z. Werb, *Nature*, 2002, **420**, 860–867.
49 X. Jin, M. A. Lee, X. Gong, V. B. Koman, D. J. Lundberg, S. Wang, N. A. Bakh, M. Park, J. I. Dong, D. Kozawa, S.-Y. Cho and M. S. Strano, *ACS Appl. Nano Mater.*, 2023, **6**, 9791–9804.
50 P. Gaikwad, N. Rahman, R. Parikh, J. Crespo, Z. Cohen and R. Williams, *bioRxiv*, 2023, preprint, DOI: **10.1101/2023.05.10.540217**.
51 R. Nißler, O. Bader, M. Dohmen, S. G. Walter, C. Noll, G. Selvaggio, U. Groß and S. Kruss, *Nat. Commun.*, 2020, 11.
52 I. T. Jolliffe and J. Cadima, *Philos. Trans. R. Soc., A*, 2016, **374**, 20150202.
53 C. Holohan, S. Van Schaeybroeck, D. B. Longley and P. G. Johnston, *Nat. Rev. Cancer*, 2013, **13**, 714–726.
54 B. Gao, S. Yeap, A. Clements, B. Balakrishnar, M. Wong and H. Gurney, *J. Clin. Oncol.*, 2012, **30**, 4017–4025.
55 J. Shi, P. W. Kantoff, R. Wooster and O. C. Farokhzad, *Nat. Rev. Cancer*, 2017, **17**, 20–37.
56 Y. Dai, C. Xu, X. Sun and X. Chen, *Chem. Soc. Rev.*, 2017, **46**, 3830–3852.
57 M. Son, P. Mehra, F. T. Nguyen, X. Jin, V. B. Koman, X. Gong, M. A. Lee, N. A. Bakh and M. S. Strano, *ACS Nano*, 2023, **17**, 240–250.
58 R. Stupp, W. P. Mason, M. J. Van Den Bent, M. Weller, B. Fisher, M. J. Taphoorn, K. Belanger, A. A. Brandes, C. Marosi and U. Bogdahn, *N. Engl. J. Med.*, 2005, **352**, 987–996.
59 V. B. Koman, N. A. Bakh, X. Jin, F. T. Nguyen, M. Son, D. Kozawa, M. A. Lee, G. Bisker, J. Dong and M. S. Strano, *Nat. Nanotechnol.*, 2022, **17**, 643–652.
60 J. T. Pinto and A. J. Cooper, *Adv. Nutr.*, 2014, **5**, 144–163.
61 M. A. Lee, F. T. Nguyen, K. Scott, N. Y. L. Chan, N. A. Bakh, K. K. Jones, C. Pham, P. Garcia-Salinas, D. Garcia-Parraga, A. Fahlman, V. Marco, V. B. Koman, R. J. Oliver, L. W. Hopkins, C. Rubio, R. P. Wilson, M. G. Meekan, C. M. Duarte and M. S. Strano, *ACS Sens.*, 2019, **4**, 32–43.
62 A. Ando, M. Hatori, Y. Hagiwara, S. Isefuku and E. Itoi, *Upsala J. Med. Sci.*, 2009, **114**, 46–51.
63 J. M. Anderson, A. Rodriguez and D. T. Chang, Foreign body reaction to biomaterials, in *Seminars in Immunology*, Academic Press, 2008, vol. 20, No. 2, pp. 86–100.
64 S.-H. Lee, D. Lee, M. H. Choi, J.-H. Son and M. Seo, *Anal. Chem.*, 2019, **91**, 6844–6849.
65 C. Grazon, R. C. Baer, U. Kuzmanović, T. Nguyen, M. Chen, M. Zamani, M. Chern, P. Aquino, X. Zhang, S. Lecommandoux, A. Fan, M. Cabodi, C. Klapperich, M. W. Grinstaff, A. M. Dennis and J. E. Galagan, *Nat. Commun.*, 2020, 11.
66 S. Yeasmin, A. Ullah, B. Wu, X. Zhang and L.-J. Cheng, *ACS Appl. Mater. Interfaces*, 2023, **15**, 13971–13982.
67 R. M. Torrente-Rodríguez, J. Tu, Y. Yang, J. Min, M. Wang, Y. Song, Y. Yu, C. Xu, C. Ye and W. W. IsHak, *Matter*, 2020, **2**, 921–937.
68 M. A. Lee, S. Wang, X. Jin, N. A. Bakh, F. T. Nguyen, J. Dong, K. S. Silmore, X. Gong, C. Pham, K. K. Jones, S. Muthupalani, G. Bisker, M. Son and M. S. Strano, *Adv. Healthcare Mater.*, 2020, **9**, 2000429.
69 P. Bouchard, *J. Reprod. Med.*, 1999, **44**, 153–157.
70 J. D. Graham and C. L. Clarke, *Endocr. Rev.*, 1997, **18**, 502–519.

71 S. E. Bulun, Y.-H. Cheng, P. Yin, G. Imir, H. Utsunomiya, E. Attar, J. Innes and J. J. Kim, *Mol. Cell. Endocrinol.*, 2006, **248**, 94–103.
72 A. D. Bannerman, X. Li and W. Wan, *Acta Biomater.*, 2017, **58**, 376–385.
73 A. Vedadghavami, F. Minooei, M. H. Mohammadi, S. Khetani, A. R. Kolahchi, S. Mashayekhan and A. Sanati-Nezhad, *Acta Biomater.*, 2017, **62**, 42–63.
74 T. R. Hoare and D. S. Kohane, *Polymer*, 2008, **49**, 1993–2007.
75 E. Mylonakis and S. B. Calderwood, *N. Engl. J. Med.*, 2001, **345**, 1318–1330.
76 L. M. Baddour, W. R. Wilson, A. S. Bayer, V. G. Fowler Jr, I. M. Tleyjeh, M. J. Rybak, B. Barsic, P. B. Lockhart, M. H. Gewitz and M. E. Levison, *Circulation*, 2015, **132**, 1435–1486.
77 N. M. Bardhan, D. Ghosh and A. M. Belcher, *Nat. Commun.*, 2014, **5**, 4918.
78 A. H. Futerman and G. Van Meer, *Nat. Rev. Mol. Cell Biol.*, 2004, **5**, 554–565.
79 T. Hendrikx, S. Walenbergh, M. Hofker and R. Shiri-Sverdlov, *Obes. Rev.*, 2014, **15**, 424–433.
80 L. LeCureux, C. S. Cheng, J. Herbst, T. P. Reilly, L. Lehman-McKeeman and M. Otieno, *Toxicol. In Vitro*, 2011, **25**, 1934–1943.
81 T. V. Galassi, P. V. Jena, J. Shah, G. Ao, E. Molitor, Y. Bram, A. Frankel, J. Park, J. Jessurun and D. S. Ory, *Sci. Transl. Med.*, 2018, **10**, eaar2680.
82 Y. Matsumura and H. Maeda, *Cancer Res.*, 1986, **46**, 6387–6392.
83 A. K. Iyer, G. Khaled, J. Fang and H. Maeda, *Drug Discovery Today*, 2006, **11**, 812–818.
84 J. T. Robinson, G. Hong, Y. Liang, B. Zhang, O. K. Yaghi and H. Dai, *J. Am. Chem. Soc.*, 2012, **134**, 10664–10669.
85 Z. Liu, W. Cai, L. He, N. Nakayama, K. Chen, X. Sun, X. Chen and H. Dai, *Nat. Nanotechnol.*, 2007, **2**, 47–52.
86 M. Antman-Passig, E. Wong, G. R. Frost, C. Cupo, J. Shah, A. Agustinus, Z. Chen, C. Mancinelli, M. Kamel, T. Li, L. A. Jonas, Y. M. Li and D. A. Heller, *ACS Nano*, 2022, **16**, 7269–7283.
87 C. R. Jack and D. M. Holtzman, *Neuron*, 2013, **80**, 1347–1358.
88 C. R. Jack Jr, D. A. Bennett, K. Blennow, M. C. Carrillo, B. Dunn, S. B. Haeberlein, D. M. Holtzman, W. Jagust, F. Jessen and J. Karlawish, *Alzheimer's Dementia*, 2018, **14**, 535–562.
89 A. Leuzy, K. Heurling, N. J. Ashton, M. Schöll and E. R. Zimmer, *Yale J. Biol. Med.*, 2018, **91**, 291.
90 M. Manley, *Chem. Soc. Rev.*, 2014, **43**, 8200–8214.
91 D. V. Savatin, G. Gramegna, V. Modesti and F. Cervone, *Front. Plant Sci.*, 2014, **5**, 470.
92 T. T. S. Lew, V. B. Koman, K. S. Silmore, J. S. Seo, P. Gordiichuk, S. Y. Kwak, M. Park, M. C. Ang, D. T. Khong, M. A. Lee, M. B. Chan-Park, N. H. Chua and M. S. Strano, *Nat. Plants*, 2020, **6**, 404–415.
93 X. Gong, S.-Y. Kwak, S.-Y. Cho, D. Lundberg, A. T. Liu, M. K. McGee and M. S. Strano, *ACS Sens.*, 2023, **8**(11), 4207–4215.
94 M. H. Wong, J. P. Giraldo, S.-Y. Kwak, V. B. Koman, R. Sinclair, T. T. S. Lew, G. Bisker, P. Liu and M. S. Strano, *Nat. Mater.*, 2016, **16**, 264–272.
95 A. Organization, *The State of Food and Agriculture 2017: Leveraging Food Systems for Inclusive Rural Transformation*, Food & Agriculture Org., 2017.
96 S. Chakraborty and A. C. Newton, *Plant Pathol.*, 2011, **60**, 2–14.
97 H. Wu, R. Nissler, V. Morris, N. Herrmann, P. Hu, S. J. Jeon, S. Kruss and J. P. Giraldo, *Nano Lett.*, 2020, **20**, 2432–2442.
98 M. C. Ang, N. Dhar, D. T. Khong, T. T. S. Lew, M. Park, S. Sarangapani, J. Cui, A. Dehadrai, G. P. Singh, M. B. Chan-Park, R. Sarojam and M. Strano, *ACS Sens.*, 2021, **6**, 3032–3046.
99 K. Boonyaves, M. C. Ang, M. Park, J. Cui, D. T. Khong, G. P. Singh, V. B. Koman, X. Gong, T. K. Porter, S. W. Choi, K. Chung, N. H. Chua, D. Urano and M. S. Strano, *Nano Lett.*, 2023, **23**, 916–924.
100 R. Nissler, A. T. Muller, F. Dohrman, L. Kurth, H. Li, E. G. Cosio, B. S. Flavel, J. P. Giraldo, A. Mithofer and S. Kruss, *Angew. Chem.*, 2022, **61**, e202108373.
101 K. Aoki and N. Saito, *Nanomaterials*, 2020, **10**, 264.
102 V. E. Kagan, N. V. Konduru, W. Feng, B. L. Allen, J. Conroy, Y. Volkov, I. I. Vlasova, N. A. Belikova, N. Yanamala, A. Kapralov, Y. Y. Tyurina, J. Shi, E. R. Kisin, A. R. Murray, J. Franks, D. Stolz, P. Gou, J. Klein-Seetharaman, B. Fadeel, A. Star and A. A. Shvedova, *Nat. Nanotechnol.*, 2010, **5**, 354–359.
103 D. Elgrabli, W. Dachraoui, C. Ménard-Moyon, X. J. Liu, D. Bégin, S. Bégin-Colin, A. Bianco, F. Gazeau and D. Alloyeau, *ACS Nano*, 2015, **9**, 10113–10124.
104 A. A. Shvedova, A. Pietroiusti, B. Fadeel and V. E. Kagan, *Toxicol. Appl. Pharmacol.*, 2012, **261**, 121–133.
105 A. Bianco, K. Kostarelos and M. Prato, *Chem. Commun.*, 2011, **47**, 10182.
106 M. P. Monopoli, C. Åberg, A. Salvati and K. A. Dawson, *Nat. Nanotechnol.*, 2012, **7**, 779–786.
107 Y. Song, C. Tian, Y. Lee, M. Yoon, S. E. Yoon and S.-Y. Cho, *ACS Meas. Sci. Au*, 2023, **3**(6), 393–403.
108 M. Kim, D. Goerzen, P. V. Jena, E. Zeng, M. Pasquali, R. A. Meidl and D. A. Heller, *Nat. Rev. Mater.*, 2023, 1–19.